ACS APPLIED NANO MATERIALS

www.acsanm.org Article

Silk Nanoparticle Synthesis: Tuning Size, Dispersity, and Surface Chemistry for Drug Delivery

Sawnaz Shaidani, Charlotte Jacobus, Jugal Kishore Sahoo, Kristin Harrington, Hannah Johnson, Olivia Foster, Shangyuan Cui, Onur Hasturk, Thomas Falcucci, Ying Chen, Madison Fletcher, Carolynn Brooks, Gregory P. Holland, and David L. Kaplan*

Cite This: *ACS Appl. Nano Mater.* 2023, 6, 18967−18977 Read Online

ACCESS | Metrics & More | Article Recommendations | Supporting Information

ABSTRACT: Protein-based nanoparticles have gained interest for traversing different biological (e.g., systemic or microenvironmental, etc.) barriers and enabling targeted drug delivery. Silk protein-based nanoparticles are useful and versatile drug delivery systems for sustained and controlled release due to their biocompatibility, biodegradability, accessible chemistries, and ability to stabilize different drugs and other biomolecules. In the present study, silk nanoparticles (SNPs) were engineered using a nanoprecipitation technique with tight control over size (∼45−250 nm diameter) and low polydispersity index by altering variables including stirring speed, reaction bath temperature, silk molecular weight (MW), and silk concentration. Of these variables, stir speed was the most significant contributor toward particle size control. SNPs with positive or negative surface charges and decoration of SNPs with surface antigens were also demonstrated. New mechanistic insights into control of SNP size, cellular uptake using glioblastoma as a model, surface characteristics, and the entrapment of a small-molecule drug (doxorubicin) within the particles were addressed. These insights expand the potential utility of SNPs for medical, environmental, and food applications.

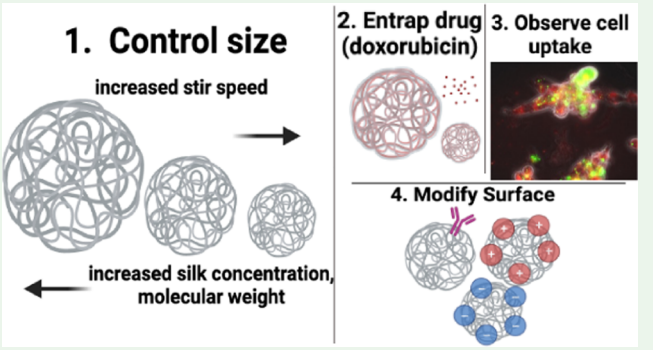

KEYWORDS: *nanoprecipitation, silk, nanoparticles, cellular uptake, nanomedicine, antibody conjugation, surface charge*

INTRODUCTION

As the field of nanomedicine advances, concerns surrounding the safety of the materials utilized have emerged. Inorganic nanoparticles such as metal-based particles have been used extensively in the literature, and several have FDA approval[1] for drug delivery, diagnostics, and imaging; however, cytotoxicity concerns including cell membrane disruption, production of reactive oxygen species (ROS), DNA damage, and release of metal ions that affect protein function prevent their wider use.[2,3] Similarly, lipid-based nanoparticles have had significant clinical success in recent years but can induce oxidative stress, acidification of the cytosol, and thus inhibition of protein synthesis *in vitro*[4] and have been reported to induce liver and lung damage *in vivo*.[5] Some of the earliest polymers used to generate nanoparticles for *in vivo* testing, such as poly(methyl methacrylate)[6] and polystyrene,[7] were not biodegradable[8] and have since been found to cause the release of proinflammatory cytokines, inducing local inflammation,[9] increased ROS[10] and lactate dehydrogenase concentrations, as well as cell-cycle arrest[10] when these materials were assessed *in vitro*[9] and *in vivo*.[8] In contrast, biodegradable polymeric nanoparticles, such as protein-based particles, have many intrinsic characteristics that make them good candidates for targeted drug delivery. Compared to conventional synthetic polymeric nanoparticles, protein-based particles can be cleaved by proteolytic enzymes[11] and broken down into amino acids, which are then metabolized or absorbed by the body.[12] The proteins can also be chemically tailored to display cell-targeting ligands or other biomolecules of interest on their surface. They can be tuned to express a positive or negative surface charge by installing appropriate chemical blocks to influence cytotoxicity and therapeutic fate.[2] Biodegradable protein-based nanoparticles can also be utilized to control the release profiles of drugs and avoid clearance by the reticuloendothelial system.[13] Protein-based particles have already begun making their way into the clinic; Abraxane, for example, is an albumin-bound particle form of paclitaxel that is widely used in the clinic,[14] and more albumin-bound particles are entering clinical trials,

Received: July 25, 2023
Accepted: September 25, 2023
Published: October 13, 2023

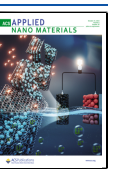

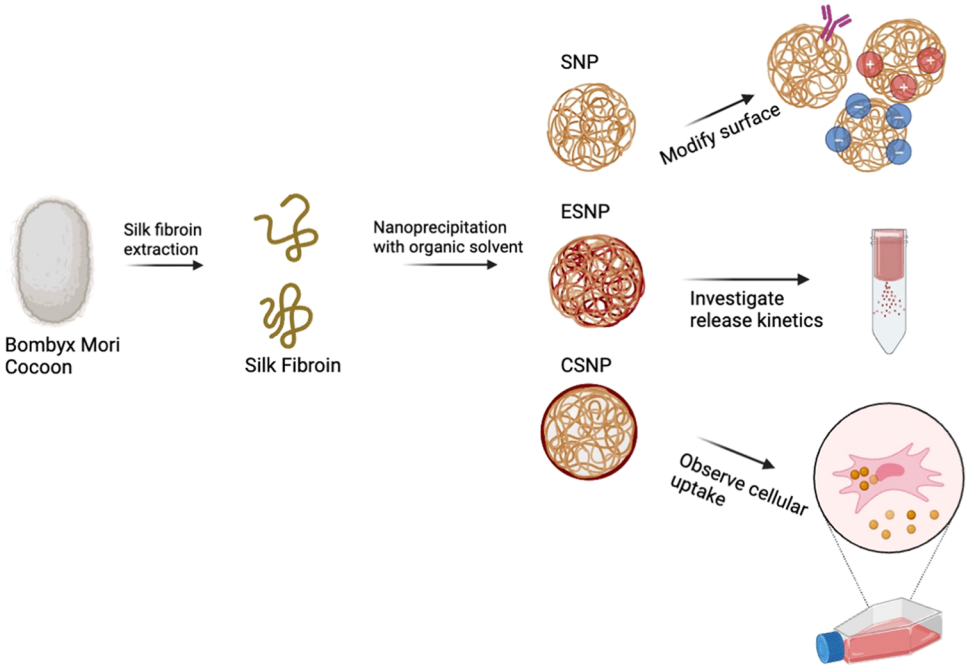

Figure 1. Schematic on the structure and applications of nanoprecipitated silk particles in this work. Silk fibroin is extracted from *B. mori* cocoons, and following particle fabrication (with or without drug, using native or positively charged silk) particles can be altered to display surface targeting agents (antibodies) and incubated with cells for cellular uptake studies. SNPs, silk nanoparticles; ESNPs, particles with entrapped drug; CSNPs, particles coated with drug. Made using BioRender.com.

highlighting the growing use of protein-based nanoparticle systems.[1]

In addition to degradability, size is an important parameter for the physical properties of nanoparticles, influencing adsorption rates, recognition by immune cells, travel through tight endothelial junctions, and filtration by the spleen, among many other factors.[15] In general, smaller particles (~80 nm) circulate in the bloodstream longer than larger particles (>200 nm).[15] In cancer therapeutics, nanoparticles can exploit the enhanced permeation and retention (EPR) effect, where the leaky vasculature of solid tumors and the weak lymphatic drainage synergistically encourage particle accumulation in target cells. In the endothelium of blood vessels of tumors, barrier distortion can result in pores; therefore, nanoparticles should be smaller than these pores (generally <200 nm) but larger than 30 nm to exploit the EPR effect, although these size ranges will depend on the cell type and material.[15−17]

Silk fibroin (hereafter referred to as silk) is biocompatible and degradable and has gained utility in drug delivery and nanoparticle research due to control of crystallinity, which impacts degradation rates, chemical structure, and assembly into materials that stabilize therapeutics that are otherwise susceptible to denaturation.[18,19] Various methods have been utilized to generate SNPs, including blending polymers such as silk-poly(vinyl alcohol) (PVA),[20] spray-drying,[21] and nanoprecipitation,[18,22] among others.[23] Nanoprecipitation or desolvation is among the most popular methods of generating SNPs in the literature and involves two miscible solutions, where the first solvent contains the polymer and the second solvent does not (the precipitation solvent). This method involves the rapid dissolution of the polymer, which induces the precipitation of nanoparticles when the polymer solution is added to the precipitation solvent.[24] This occurs due to the Marangoni effect, where the interfacial turbulence between a solvent and a nonsolvent governs particle formation.[25] One limitation of the current nanoprecipitation method is the inability to precisely control the size of the resulting nanoparticles across a broad size range.[15] In addition, the maintenance of a low polydispersity index (PDI) is essential in nanoparticle applications. Nanoprecipitation of natural biopolymers often produces particles greater than 100 nm in diameter. For example, recent works on nanoprecipitated particles prepared with naturally derived biopolymers have resulted in gelatin nanoparticles with sizes of 130−190 and 273 nm in a one-step[26] and two-step fabrication method,[27] chitosan particles with a size range of 200−≥600 nm with irregular particles formed at larger sizes,[28] and albumin nanoparticles with a size range of 90−450 nm with a broad PDI (0.02−0.8).[29]

Nanoprecipitated SNPs have been generated with a 100 nm diameter using low-molecular-weight (MW) silk and have been loaded with doxorubicin (DOX) to treat a human breast cancer cell line.[18] These SNPs colocalized into lysosomes, thus demonstrating potential for cancer treatments.[30] The particles were also biocompatible in nondrug loaded formulations.[30] However, a limitation of this method was the inability to produce SNPs across a broader size range while maintaining a low PDI. Investigation of the effect of stir rate (0, 200, and 400 rpm) during silk nanoparticle formation was also completed recently, and particles between 104 and 134 nm in diameter were generated using isopropanol as the nonsolvent.[31] There have been limited studies to date to understand how to reproducibly control nanoprecipitated SNP size and PDI, yet the effect of size on cellular uptake and drug release is key. Additionally, previous methods to generate DOX-loaded SNPs only incubated premade particles in drug solutions to provide drug coatings (adsorption) on the particles, which limits protection from the surrounding environment and prevents the addition of postfabrication surface modifications.

In the present study, nanoprecipitated SNPs were reliably and reproducibly generated over a diverse size range from ~45

https://doi.org/10.1021/acsanm.3c03451
ACS Appl. Nano Mater. 2023, 6, 18967−18977

to 250 nm while maintaining a low PDI (~0.2−0.4). Significant control over the size of the resulting SNPs was achieved by changing the silk properties (molecular weight and concentration) and reaction bath parameters (temperature and stir speed). In addition to size, the surface properties of these nanoparticles were altered by using prefunctionalized silk as starting precursor molecules or chemically appending appropriate pendant groups to the surface of the SNPs in a postfunctionalization process. SNPs of different sizes were successfully incubated with a cancer cell line (glioblastoma) as a model for the cellular uptake and investigation of these particles for oncologic applications, and the entrapment of DOX in the SNPs was also investigated (Figure 1).

MATERIALS/METHODS

Silk Isolation. Silk fibroin was isolated from *Bombyx mori* cocoons as previously described.[22] Briefly, the cocoons (Tajima Shoji Co., Japan) were boiled in a 0.02 M sodium carbonate solution for 10, 30, or 60 min to remove the sericin and achieve different molecular weights of silk, which we have previously published.[32] The extracted silk was then dried for 12 h in a chemical hood before being dissolved in a 9.3 M lithium bromide solution at 60 °C for 4 h, yielding a 20% w/v solution. This solution was dialyzed against deionized (DI) water using Pierce Slide-a-Lyzer cassettes, MWCO 3500 Da (Rockford, IL) for 3 days to remove the lithium bromide. The solution was centrifuged (9000 rpm, 4 °C, 20 min cycle), and a final concentration of the aqueous silk fibroin of ~5−10% w/v was obtained. For the 10 min extracted silk, extra rinse steps (3−5) immediately after boiling were employed to effectively remove any residual sericin, as any residual sericin prohibits particle formation.

Fabrication of SNPs. Nanoprecipitated SNPs were prepared as previously published but with modifications.[18,22] Briefly, a 5−10% w/v silk solution was added dropwise using a 60 mL addition funnel (Fisherscientific CG170401, Waltham, MA) at a drop length of 7 cm and a drop rate of approximately 8−10 drop/min to acetone while stirring (200 rpm −1,200 rpm, Cole Palmer UX-84003−80, Vernon Hills, IL) with a 15 mm × 4 mm stir bar to create a cloudy solution that was >75% v/v acetone (typically, 3.5−4 mL of silk solution was added to ~17.5−18 mL of acetone in a 20 mL scintillation vial). Cold bath particles were prepared by adding a 6% (w/v) silk solution dropwise to −20 °C acetone while stirring at 800 rpm. The nanoparticle suspension was allowed to stir for 48−72 h to evaporate all of the solvent. The nanoparticle suspension was then diluted with deionized water and sonicated with a Branson Ultrasonic Cell Disruptor for 30 s at 30% amplitude. For each experiment, nanoparticles were prepared in replicates (typically in at least triplicate unless otherwise stated), where different batches of silk were dissolved to generate each nanoparticle suspension replicate. To make fluorescently labeled SNPs, fluorescein isothiocyanate (FITC) was dissolved in dimethyl sulfoxide (DMSO) to achieve a 10 mg/mL solution. Per 100 mg of silk solution needed for the nanoprecipitation process, 1 mg of FITC was added (e.g., for 4 mL of a 5% w/v silk solution, 200 uL of the FITC stock solution was added to add 2 mg of FITC to 200 mg of silk). After adding the FITC to the silk solution and ensuring homogeneous mixing, the nanoprecipitation process was conducted. Any unbound FITC was dialyzed and/or ultracentrifuged at 60,000 rpm, 4 °C, for 30 min (Beckman Coulter Optima Max TL with TLA-110 rotor, Brea, CA) from the SNPs with several wash cycles until the supernatants revealed no leached or unbound FITC using a plate reader (491 nm excitation and 516 nm emission, Varioskan ThermoFisher, Waltham, MA).

Size Quantification. The size, PDI, and ζ-potential of the SNPs were measured by using a ZetaPALS dynamic light scattering (DLS) machine (Brookhaven Instruments, Holtzville, NY). Of note, size and PDI measurements were taken 3 times on the DLS machine for each sample (technical replicates) and then averaged for each batch of SNPs dissolved from a fresh batch of silk (biological replicates). Because of this, the variability of sizes may be higher than the variability of the PDI between different biological replicates. To verify the readings, scanning electron microscopy (SEM) and transmission electron microscopy (TEM) were utilized. For SEM, the nanoparticles were coated with a thin layer (10 nm thick) of Pt/Pd using a sputter coater (208HR, Cressington Scientific Instruments Inc.) and imaged (Zeiss UltraPlus SEM or Zeiss Supra 55 VP SEM, Carl Zeiss SMT Inc.) at a voltage of 3 kV.

For TEM, 2% ammonium molybdate stain was prepared, and the pH was adjusted to 6.9 using sodium hydroxide. The stain was filtered through a 0.2 μm filter just before use. Carbon-coated Cu grids (Ted Pella, Inc., 400 mesh size, Redding, CA) were glow-discharged for 30 s using a PELCO easiGlow. All grids were prepared within 30 min of glow discharge. Five μL of sample was pipetted directly onto the grid for 30 s before blotting using a filter paper (Whatman 1. Thermofisher, 09805F, Waltham, MA). The grid was immediately placed on a 50 μL drop of 2% ammonium molybdate, pH 6.9, for 15 s before blotting. This staining step was repeated twice, with blotting between each step. After the final blot, the filter paper was pressed to the edge of the grid near the tweezers to remove excess stain. Grids were dried sample side down on a filter paper overnight. Images were collected on a Tecnai T12 in the San Diego State University Electron Microscope facility at 120 kV and spot size 3 using a side-mounted CCD camera.

Cell Culture, Uptake, and Staining. U87-MG (ATCC HTB-14 Manassas, VA) glioblastoma cells were cultured in Dulbecco's modified Eagle's medium (DMEM)-F12 supplemented with 1% antibiotic-antimycotic (Sigma-Aldrich) and 10% fetal bovine serum (FBS).

For live cell imaging, 100,000 cells/well were seeded in 6-well plates and left to recover for 2 days. Media containing FITC-labeled particles was added at 16.5 μg/mL for 4 h. The media was then aspirated, and media containing Lysotracker Deep Red (ThermoFisher, L12492, Waltham, MA) was incubated with the cells for 30−40 min according to the manufacturer's instructions. Lysotracker medium was aspirated, and fresh medium was added to the wells. Trypan blue dye was added to the wells in a 1:2 ratio of Trypan blue to media to quench the fluorescence from extracellular particles and visualize only intracellular FITC-tagged particles. Cells were imaged on a Keyence all-in-one fluorescent microscope (BZ-X710, Keyence Corp, Japan) within 30 min of the addition of Trypan blue. Explanations of imaging controls to ensure only intracellular SNPs are visualized are detailed in the Supporting Information. All images shown were taken at the same exposure levels.

For fixed cell imaging, similar methods were employed. Here, 100,000 cells/well were seeded in 6-well plates and left to recover for 2 days. Media containing FITC-labeled particles was added at 16.5 μg/mL for 4 h. U87-MG cells were fixed with 4% paraformaldehyde for 30 min, permeabilized with 0.1% Triton X-100 at room temperature (RT) in 1% blocking buffer (Abcam, ab210904, Waltham, MA) for 10 min, and blocked with 1% blocking buffer for 45 min to 1 h. The permeabilized cells were incubated with an antibody for lysosome-associated membrane glycoprotein 2 (LAMP2, Thermofisher PA1655, Waltham, MA) overnight at 4 °C while shaking and then the early endosome antibody EEA1 (Thermofisher MA514794, Waltham, MA). To visualize if the particles were in locations other than the endosomes and lysosomes, the same secondary antibody (labeled with AlexaFluor 405, Thermofisher, A31556, Waltham, MA) was used for both as both primary antibodies utilized rabbit hosts. Incubation of the secondary antibody was conducted in the dark with shaking at RT. Finally, phalloidin was added according to the manufacturer's instructions for 30 min at RT in the dark with shaking (labeled with AlexaFluor 555, Thermofisher, A34055, Waltham, MA). All dilutions of the antibodies were done according to the manufacturer's instructions (LAMP2−1:20, EEA1−1:100, secondary antibody labeled with AlexaFluor 405−1:200, phalloidin −1:200). Between the sequential staining steps, the samples were washed in phosphate buffered saline (PBS) containing 0.1% Tween-20. Images were taken within 24 h of staining using a Leica SP2 confocal microscope (Leica Microsystems) and a Nikon A1R (Nikon Instruments Inc.) with Z-series capability. Images were

https://doi.org/10.1021/acsanm.3c03451
ACS Appl. Nano Mater. 2023, 6, 18967−18977

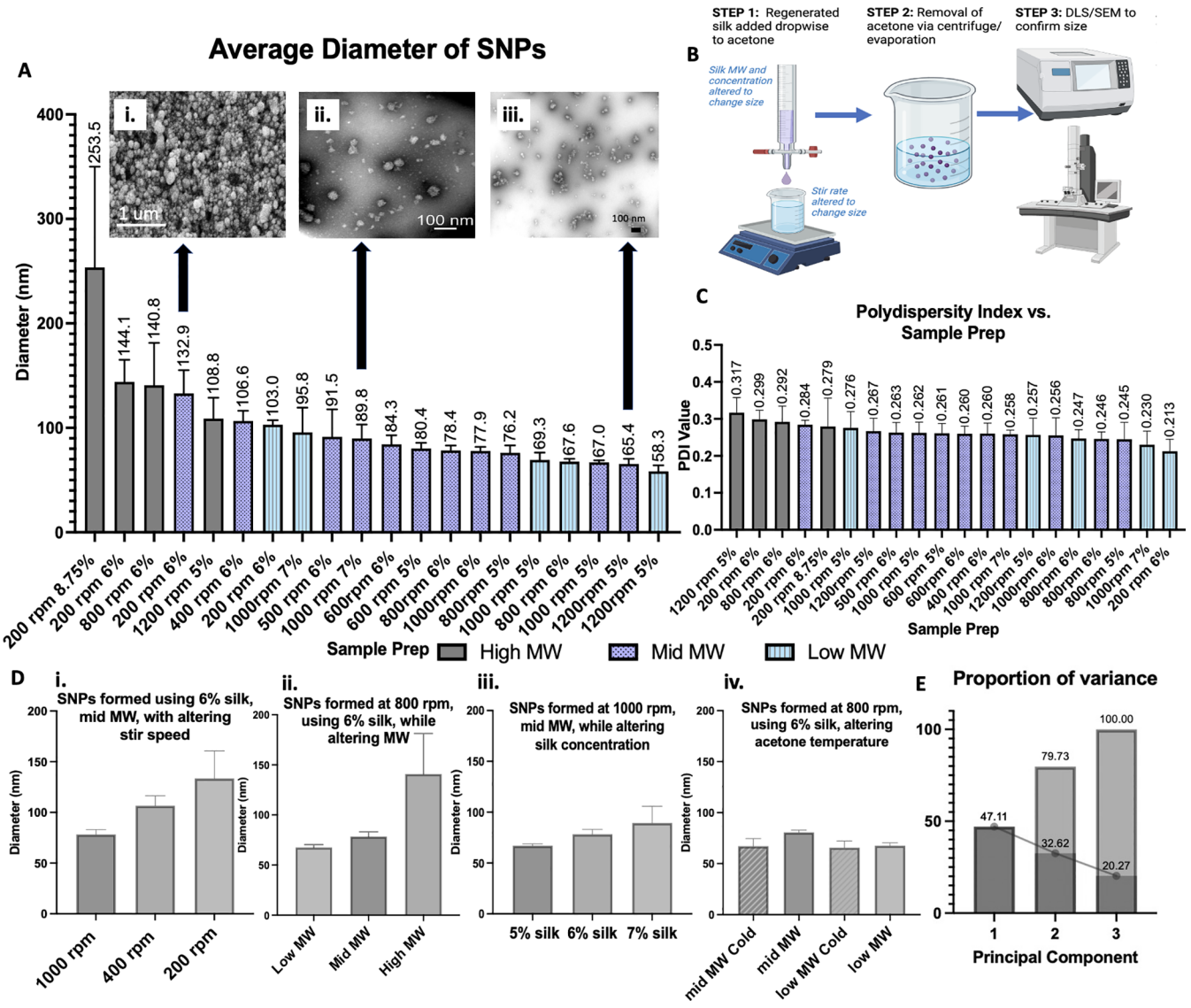

Figure 2. Control of SNP size. (A) Average diameter of SNPs fabricated with different formulation methods using dynamic light scattering (DLS). (i) SEM of 130 nm particles formed at 200 rpm, 6% silk, mid-MW. (ii) TEM images of 90 nm particles, formed using 1000 rpm stir speed, 7% silk, and mid-MW. (iii) TEM images of 65 nm particles, formed using 1200 rpm stir speed, 5% silk, and mid-MW. Sizes of technical replicates were averaged and then graphed for each biological replicate (see Methods; $n \geq 3$ biological replicates). (B) Nanoprecipitation protocol, where silk solution is added dropwise to an acetone bath, with a specific silk concentration, MW, and stir rate, followed by removing acetone, and then characterization. (C) PDI of SNPs of various sizes, using different formulation combinations seen in (A) by DLS. PDIs of technical replicates were averaged and then graphed for each biological replicate (see Methods, $n \geq 3$ biological replicates). (D) (i) Particles formed using the same concentrations and MWs, but different stir speeds. (ii) Particles formed using different silk MWs. (iii) Particles formed using the same stir speed and MW, but different concentrations. (iv) Nanoprecipitation performed at colder temperatures to induce size differences while maintaining the molecular weight, concentration, and stir speeds. (E) PCA of the variables: PC1, stir speed; PC2, concentration; PC3, molecular weight. 60 min extraction: low MW (<171 kDa); 30 min extraction: mid-MW (31−268 kDa); and 10 min extraction: high MW (171−460 kDa).[32] Error bars represent standard deviation, $n \geq 3$.

assembled with Leica confocal software (ver 2.61, Leica), NIS-Elements AR software package (ver 4.20.01, Nikon), and ImageJ.

Drug Loading and *In Vitro* Release Profile. To entrap DOX in the SNPs, the drug was added directly to the silk solution prior to nanoprecipitation (ESNPs). Briefly, a 10 mg/mL solution of DOX was generated in DMSO, and 200 μL of this solution (2 mg) was added to 4 mL of a silk solution used for nanoprecipitation. Immediately following nanoprecipitation of the ESNPs, the silk−acetone−doxorubicin mixture (21−22 mL) was ultracentrifuged (3×, 60,000 rpm, 30 min, 4 °C) to remove unbound DOX and acetone. Supernatants were saved each time for the quantification of loading. To coat the SNPs with DOX (CSNPs), similar protocols were used with modifications[18] to compare the ESNPs to the CSNPs. Using one batch of premade, unloaded SNPs, 200 μL (2 mg) of DOX stock solution (DMSO) was added, and the volume was brought to 21−22 mL using distilled water and left to incubate overnight at RT while stirring. After the overnight incubation for CSNPs, the particles were ultracentrifuged 3×, 60,000 rpm, 30 min, 4 °C to remove unbound DOX, and the supernatants were again saved for quantification of loading.

For the *in vitro* release profile, 500 μL of either ESNPs or CSNPs suspended in PBS was pipetted into Slide-A-Lyzer 3.5K mini dialysis devices (ThermoFisher, PI69550, Waltham, MA), which were suspended in 1.8 mL of phosphate buffer pH 7.4, at 37 °C. The 1.8 mL was saved for DOX quantification at each time point and replaced with fresh PBS. These experiments were done with three

https://doi.org/10.1021/acsanm.3c03451
ACS Appl. Nano Mater. 2023, 6, 18967−18977

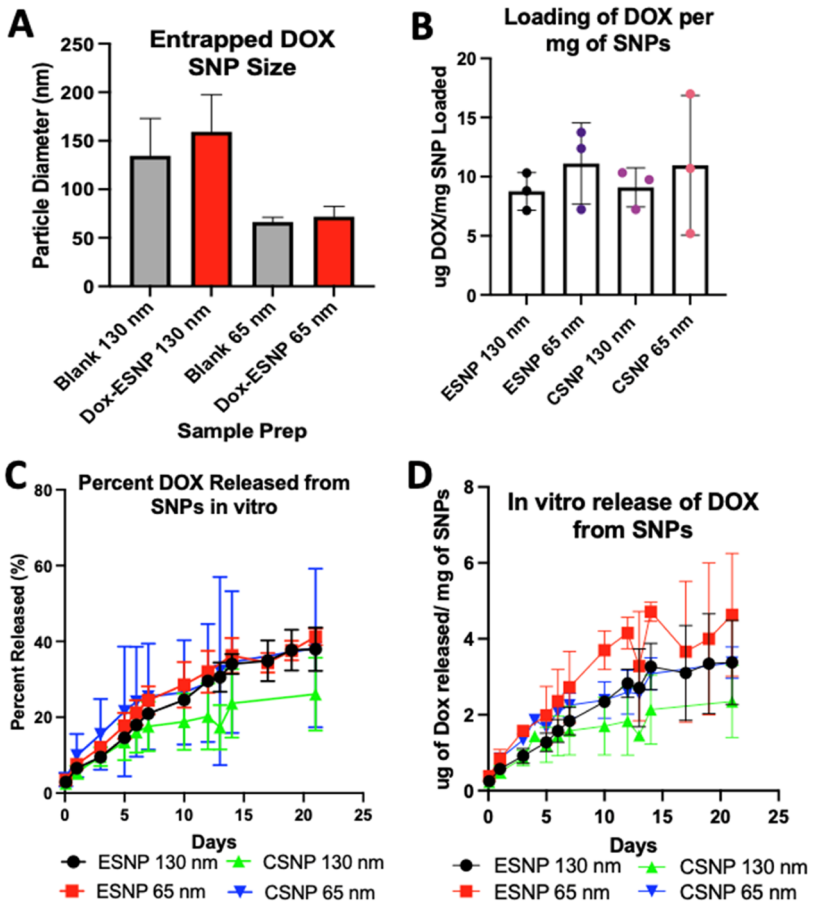

Figure 3. Doxorubicin loading into SNPs, and release profiles. (A) Size differences in blank, unloaded particles *vs* particles with predissolved doxorubicin prior to nanoprecipitation (entrapment, ESNP). (B) Loading of doxorubicin in entrapped drug SNPS (ESNPs) *vs* particles coated with doxorubicin (CSNPs) per mg of SNPs. (C) Percent doxorubicin released in the entrapped drug SNPS (ESNPs) *vs* particles coated with doxorubicin (CSNPs) over time. (D) *In vitro* release profile of doxorubicin from ESNPs of different sizes compared to CSNPs. Error bars represent standard deviation, $n = 3$.

technical replicates per experiment, with three separate experiments (new batch of the ESNPs or CNSPs derived from freshly degummed silk), using two conditions: the 200 rpm, 6% w/v silk, 30 min extraction (mid-MW) formulation, and the 1200 rpm, 5% w/v silk, 30 min extraction (mid-MW) formulation.

The amount of DOX in the release samples was quantified with high-performance liquid chromatography (HPLC, Agilent Technologies) using previously established methods.[33] Briefly, an Agilent ZORBAX Eclipse Plus-C18 column (5 μm, 3 × 150 mm^2) was used with a mobile phase of acetonitrile and water (32:68, v/v) that was pH-adjusted to 2.6 using 85% orthophosphoric acid. The mobile phase was administered isocratically at a flow rate of 1 mL/min at 35 °C. Samples were read at 475 nm excitation and 555 nm emission wavelengths with an injection volume of 50 μL.

Positively Charged Particles. To generate cationic SNPs, silk was carbodiimide-coupled with ethylenediamine (EDA) using 1-ethyl-3-(3-(dimethylamino)propyl) carbodiimide/*N*-hydroxy succinimide (EDC/NHS) bioconjugation chemistry. EDC and NHS were weighed, and 0.2 M 2-(*N*-morpholino)ethanesulfonic acid (MES) buffer (pH 6) was added to reach a final reaction concentration of 0.05 M as previously described.[34] Silk, MES buffer, EDC, NHS, and EDA were combined and stirred at 200 rpm for 18 h at RT. The silk solution was dialyzed for 72 h to remove the unbound EDA and other byproducts, followed by centrifuging (9000 rpm, 20 min, 4 °C) to remove silk debris as previously described.[34] The nanoprecipitation protocol was then carried out using the cationic silk directly after chemical modification by concentrating to the appropriate concentration or using lyophilized cationic silk that was reconstituted in deionized (DI) water to yield positively charged SNPs.

Antibody Conjugation. Antibody conjugation was conducted similarly to previously reported methods of attaching antibodies to silk films.[35] EDC and NHS were weighed, and 0.05 M MES buffer (pH 6) was added similarly to previously described protocols.[34] Briefly, 12.4 mg of EDC and 4 mg of NHS were dissolved in 0.05 M MES buffer (pH 6) and brought to 2.4 mL with 5 mg of SNPs (200 rpm, 6% silk, and mid-MW formulation). Then, 10 μg of primary antibody (anti-epidermal growth factor receptor (EGFR), MA5–13319, Thermofisher Waltham, MA) was added to the MES, EDC/NHS, and SNP mixture and stirred at 200 rpm for 18 h. The next day, this mixture was ultracentrifuged at 60,000 rpm for 30 min at 4 °C to pellet the particles. The pellet was resuspended in DI water and spun down 2 more times to wash. The particles were then resuspended in 3 mL of DI water, containing 0.2% blocking buffer (10×, Abcam, ab210904) and 0.01 mg/mL secondary antibody AlexaFluor 405, A-31553, Thermofisher, Waltham, MA for 2 h shaking at RT. Blank SNPs were also incubated in 0.2% blocking buffer and 0.01 mg/mL secondary antibody as a control for nonspecific binding of the secondary antibody to the SNPs. The fluorescence of the particle aggregates was read using the Varioskan LUX Multimode Microplate Reader (401 nm excitation, 426 emission), and the particles were imaged on a Keyence all-in-one fluorescent microscope. ESNPs (200 rpm, 6% silk, and mid-MW formulation) were also tested for antibody conjugation of anti-EGFR for determination of successful antibody binding after drug loading. In order to observe potential loss of doxorubicin and changes in doxorubicin fluorescence from the particles after antibody conjugation processes, the fluorescence of the particle aggregates was read using the Varioskan LUX multimode

https://doi.org/10.1021/acsanm.3c03451
ACS Appl. Nano Mater. 2023, 6, 18967−18977

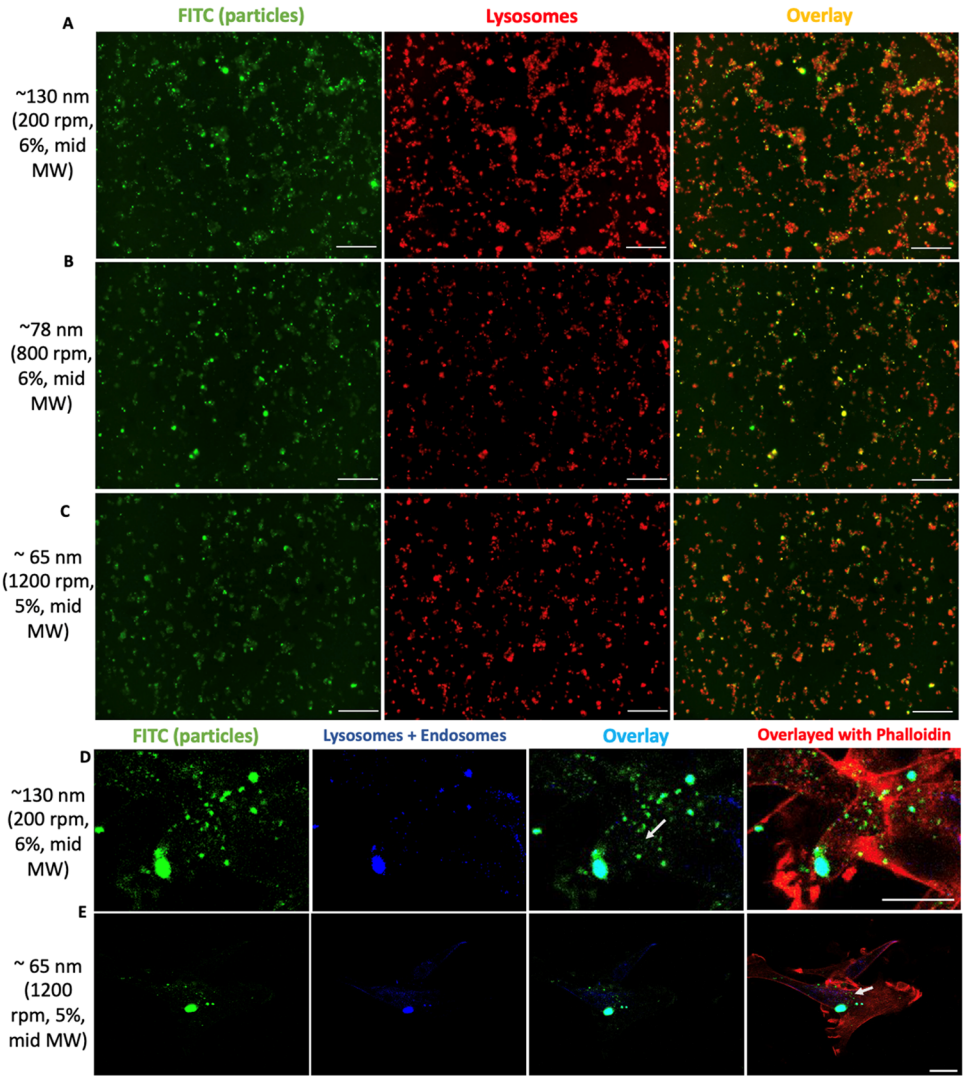

Figure 4. Cellular uptake of SNPs. (A–C) Live cell imaging of fluorescently (FITC, green) tagged nanoparticles 130 nm (A), 78 nm (B), or 65 nm (C) in U87-MG glioblastoma cells with stained lysosomes (Lysotracker, red). Overlayed images show colocalization of particles with the lysosomes in orange/yellow. Scale bar is 200 μm; images were taken in 10× with the same exposure levels, $n \geq 3$. (D, E) Confocal, fixed imaging of fluorescently (FITC, green) tagged nanoparticles that are 130 nm (D) or 65 nm (E) in U87-MG glioblastoma cells with stained lysosomes (Lamp2, blue), early endosomes (EEA1, blue), and phalloidin (red). Colocalization of the particles with endosomes/lysosomes is indicated in cyan, and colocalization of SNPs with the cytoskeleton (phalloidin) is shown in yellow. Arrows indicate potential areas where particles do not colocalize with any labeled regions. Scale bar is 20 μM; images are 40×. $n \geq 3$.

microplate reader (470 nm excitation, 560 nm emission) before and after conjugation.

Statistical Analysis and Principal Component Analysis. All data are expressed as mean ± standard deviation. GraphPad Prism (GraphPad Software, La Jolla, CA) was used to perform one-way analysis of variance (ANOVA) with Tukey's multiple-comparison post hoc test for most purposes unless otherwise stated. Principal component analysis (PCA) was utilized to determine the variables that contributed most to altering the nanoparticle size. The data were standardized, and a covariance matrix was computed. The eigenvalues and eigenvectors of that matrix were computed to identify the principal components of the data set. The percentage of variance in the data that can be explained by a single principal component was calculated. For each experiment, unless otherwise stated, nanoparticles were evaluated in at least triplicate, where different batches of silk were dissolved to generate the nanoparticles for each "biological" replicate. Meaning, each "n" was evaluated by using a freshly made batch of SNPs. Each biological replicate also had technical replicates.

RESULTS

Controlling the Size of SNPs and PDI of SNPs. SNPs of various sizes were synthesized *via* nanoprecipitation techniques (Figure 2A,B). All particles generated had a PDI between ~0.2 and 0.32 (Figure 2C), which was independent of size. Decreasing the stir speed (Figure 2D(i)) while increasing the silk molecular weight (Figure 2D(ii)) and concentration (Figure 2D(iii)) led to larger particle sizes, while decreasing the silk concentration and molecular weight and increasing the stir speed resulted in smaller particle sizes. Further, when more vigorous magnetic stirring was used, thus increasing shear forces, smaller particles formed (Figure S1). When particles were formed in chilled (−20 °C) acetone, smaller particles generally formed (Figure 2D(iv)). From PCA analysis (Figure 2E), the stir speed of the acetone bath during nanoprecipitation of the particles accounted for 47.11%, the weight percent of silk accounted for 32.62%, and the molecular weight of the silk accounted for 20.27% of the variance in particle

https://doi.org/10.1021/acsanm.3c03451
ACS Appl. Nano Mater. 2023, 6, 18967−18977

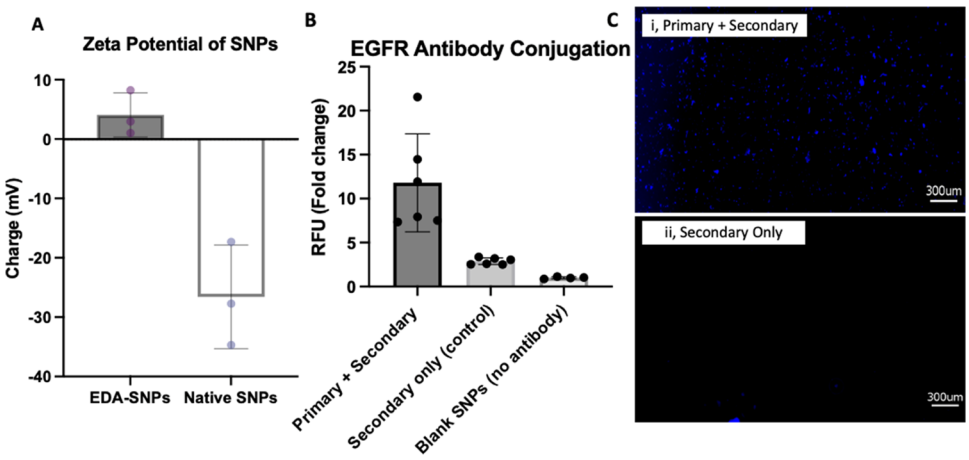

Figure 5. Enhancement of the material properties of SNPs. (A) Altered ζ-potential after amination of the silk solution prior to nanoprecipitation to generate a positive surface charge in comparison to native (unmodified) silk nanoparticles (n = 3). (B) Relative fluorescent units (RFUs) of the fluorescent secondary antibody attached to the primary antibody conjugated to the surface of the SNPs, compared to nonspecific binding in the "only secondary control" (n = 2 for this antibody, all technical replicates plotted). All values were normalized against the blank SNPs. (C) (i) Fluorescent NP aggregates after secondary antibody incubation with conjugated NPs compared to (ii). Nonspecific binding of blank particles incubated with a secondary antibody, without the primary antibody conjugated to the surface (n = 2). Error bars represent standard deviation. Scale bar is 300 μm. Exposure levels used to take images were the same for all images.

diameter. As mentioned, different molecular weights were achieved *via* extraction (boiling) times, which we have previously published—60 min extraction: low MW (<171 kDa); 30 min extraction: mid-MW (31−268 kDa); and 10 min extraction: high MW (171−460 kDa).[32]

Doxorubicin-Loaded SNPs. Doxorubicin predissolved in silk solution prior to nanoprecipitation yielded particles of similar sizes as the unloaded particles, indicating that DOX can be entrapped within SNPs and maintain a similar particle size control as established in Figure 2 (Figure 3A). Differences in loading occurred when the same amount of doxorubicin (2 mg) was added to each batch of SNPs (Figure 3B); smaller particles demonstrated higher amounts of DOX loaded per milligram of SNPs (CSNP: 10.96 ± 5.906 μg/mg, ESNP: 11.11 ± 3.436 μg/mg) than larger particles (CSNP: 9.09 ± 1.653 μg/mg, ESNP: 8.751 ± 1.586 μg/mg). In both systems, particles released DOX over 21 days (Figure 3C,D). Particles formed using the smaller particle formulation (1200 rpm, 5% w/v silk concentration, and mid-MW) released more DOX per milligram of SNPs. After 21 days, 37.96% ± 5.7 and 41.22% ± 2.2 of DOX initially loaded had been released from the ESNP 130 nm and ESNP 65 nm samples, respectively, while 26.10% ± 9.6 and 38.26% ± 20.93 released from the CSNP 130 nm and CSNP 65 nm samples, respectively (Figure 3C).

Cellular Uptake of SNPs of Different Sizes. For cellular uptake, the particles were taken up into glioblastoma cells after 4 h of incubation (Figure 4A−C). In both live and fixed cellular uptake experiments, the particles colocalized to the lysosomes and/or endosomes (Figure 4A−C, colocalization = red/yellow; Figure 4D,E colocalization = cyan); however, nanoparticles also seemed to be located in areas that did not colocalize with the endosomes, lysosomes, or the cytoskeleton of the cells, which would have been indicated by phalloidin/FITC overlap (Figure 4D,E, colocalization = yellow). This result suggests that there were particles escaping the endosomes or lysosomes but are still in intracellular locations; however, this observation could be a fixation or immunostaining artifact. Confirmation of intracellular uptake *via* appropriate controls for live cell imaging was done by quenching any extracellular FITC using Trypan Blue. Confirmation of intracellular uptake for confocal, fixed cell imaging was accomplished *via* observations of areas that did not colocalize with phalloidin. Intracellular visualization of larger SNPs (130 nm) was more pronounced at the 4 h time point than for the smaller SNPs (78 or 65 nm) based on both live and fixed cell imaging.

Modification of Material Properties: Charge and Antibody Conjugation of SNPs. Unmodified SNPs have been reported to exhibit a ζ-potential as low as −49 mV.[18] By using EDA-modified silk,[34] nanoparticles were fabricated to express a positive surface charge (Figure 5A), since EDA incorporation increased the primary amine content in silk.[34] EDC coupling mechanisms have previously supported surface immobilization of antibodies on other silk-based heterogeneous material formats like films;[35] however, here, the goal was to couple antibodies to nanoprecipitated SNPs. Thus, a primary antibody was coupled to the SNPs using EDC/NHS carbodiimide coupling chemistry, and the covalent incorporation of the antibody was validated using a fluorescent secondary antibody. In comparison to SNPs incubated in a secondary antibody solution without primary antibody conjugation (control), SNPs with the primary antibody previously conjugated showed a significantly higher fluorescence intensity (Figure 5B,C) to support the successful conjugation of the primary antibody to the surface of the SNPs. Any fluorescence expressed by the SNPs incubated in a secondary antibody solution without the primary antibody conjugation (Figure 5C(ii)) demonstrates nonspecific binding as a control. We also repeated the same experiment for ESNPs and found that while less antibody was able to be conjugated than the nondrug loaded particles, the anti-EGFR conjugated ESNPs showed a significantly higher fluorescence intensity than the controls (Figure S2) without inducing changes of DOX fluorescence by the SNPs from the conjugation process.

DISCUSSION

Silk Particle Size Controlled by Molecular Weight, Concentration, Temperature, and Stir Rate. Several

https://doi.org/10.1021/acsanm.3c03451
ACS Appl. Nano Mater. 2023, 6, 18967−18977

variables, either having precursor properties like MW and concentration or reaction bath conditions (temperature, stirring speed), were altered to assess their impact on the size of the resulting nanoparticles. Silk is shear-responsive[36] and crystallizes when shear forces are applied. Additionally, water-miscible organic monohydric solvents such as methanol and ethanol or polar solvents such as acetone increase the crystallinity in silk materials by accelerating β-sheet structure formation.[37] We hypothesized that combining shear forces induced by an increased magnetic stirring rate and maintaining exposure to organic solvents would increase the crystallization rate of silk, thus resulting in smaller particles. Stirring also decreased silk chain aggregation, supporting a lower PDI. Further, silk is also temperature-responsive and crystallizes more rapidly at higher temperatures.[38] We hypothesized that cooling the acetone bath would result in a slower silk aggregation, resulting in particles smaller than those of the process run at RT.

Silk nanoprecipitation is governed by the shift of water molecules away from the hydration shell of silk.[39] Based on previous studies,[40] we hypothesized that more efficient and rapid "ripping" of the water molecules away from the silk hydration shell by magnetic stirring would generate smaller particles and that this could be expanded with a broader range of stir speeds. Lower MW silk was expected to generate smaller-sized particles.[32] We also hypothesized that lower concentrations of silk would result in the formation of smaller particles, as decreasing silk content while keeping the acetone volumes constant would likely result in reduced exposure of silk hydration shells to the acetone.

Altering SNP Features. Protein-based nanoparticles have many characteristics that are advantageous for targeted drug delivery. Accessible chemistries, imparted by the presence of many chemically active amino acids, are one of them. They can be easily chemically modified using many established routes to display cell-targeting ligands on their surface[41] and can be tuned to display a positive or negative surface charge by functionalization with appropriate ligands.[41] *In vivo*, these surface charges will change due to the protein corona formed around the particles, which describes the layer of proteins in physiological fluids that assemble on the surface of nanoparticles.[42] This protein layer is governed by the physicochemical properties of the nanoparticle, such as surface charge and hydrophobicity.[42] With protein-based particles like silk, the surface charge and degree of hydrophobicity can be readily tuned, allowing for potential future control of the protein corona *in vivo*.[34,41,43] Tuning the surface charge of SNPs is advantageous for the intracellular delivery of active pharmaceutical agents, as charge can affect the serum proteins absorbed onto the surface of the particles and thus the cellular uptake and as cells are slightly negatively surface charged.[44] Additionally, positively charged particles can support coatings of negatively charged polymers such as alginate and negatively charged antigens or drugs to bind to the surface of the nanoparticles *via* electrostatic interactions.

Prior to this research, a significant limitation with silk nanoparticles formed *via* nanoprecipitation was a lack of size control across a broad size range while maintaining a low PDI and particle morphology.[18,45] This was also the case for other biopolymers, as mentioned (gelatin,[26,27] chitosan[28]). In the present study, we demonstrated the expansion of processing parameters to generate reproducible NPs with a wider range of specific sizes using nanoprecipitation while also maintaining a tight PDI. This control and insight should support new opportunities to utilize such defined and functionalized SNPs in new targeting applications. Control of particle size using similar principles has been reported in spider silks;[46,47] however, extensive size control with particles <200 nm has not been established to our knowledge with spider silks.

Understanding how size affects drug release kinetics is critical, and here, the release of doxorubicin from the 65 nm SNPs was more rapid in comparison to the 130 nm SNPs. This difference was expected, due to the higher surface-to-volume-ratio of the smaller particles, which would induce more rapid release of the DOX out of the smaller particles.[48−50] We also showed differences in loading between the smaller and larger particles, possibly due to the silk content used to formulate the particles, as the 65 nm formulation utilized 5% w/v silk and the 130 nm formulation utilized 6% w/v silk. Additionally, there was increased variability in the loading and the percent of DOX released in the CSNPs over time in comparison to the ESNPs, suggesting that the entrapment of DOX rather than coatings (adsorption) leads to a more reproducible release profile and loading. As mentioned, an advantage of polymeric nanoparticles is the ease of attaching cell-targeting ligands on their surface, yet the postprocessing conditions required to attach these ligands can lead to the loss of drug coatings. Drug coatings may block the targeting ligands from adhering to the surface of the SNPs. Drug coatings on NPs can also result in premature loss of drug before reaching the target site *in vivo*, which in the case of chemotherapy would cause harm to healthy tissues and insufficient cell death in the target (cancerous) tissue. Entrapment of DOX within SNPs, rather than as a coating, therefore, has the potential to protect the chemotherapy drugs during the postprocessing conditions. Although there was decreased antibody conjugation demonstrated in ESNPs than nondrug loaded SNPs, we showed that anti-EGFR was still able to attach successfully in comparison to controls. The decreased antibody conjugation to the ESNPs in comparison to the SNPs was expected, as DOX−silk interactions likely are also present on the surface of ESNPs, decreasing the available area for the conjugation to occur in comparison to nondrug loaded particles. Additionally, other methods to produce silk-based NPs with chemotherapy drugs entrapped within the particles mostly utilize sizes larger than 300 nm, thus rendering them less useful for cellular uptake.[51] Therefore, we successfully generated SNPs where the DOX was added to the silk prior to generating the particles to efficiently entrap the drug while not significantly altering the particle sizes and resulting in sustained *in vitro* release over 20 days. While this release profile would not be observed at a cellular level as the particles will likely be destroyed in the lysosomes of the cells resulting in immediate drug release, this sustained release profile could be useful for other drug delivery systems where SNPs are embedded within other materials such as hydrogels or spongy scaffolds.

For internalization of nanoparticles by the cells, endocytic mechanisms (pinocytosis, endocytosis) depend on size and surface properties.[52] After internalization, nanoparticles are typically transported from the early endosome to the late endosome and then to the lysosomes to be disrupted. For delivery of mRNA, nanoparticles must escape the endosome or lysosome and enter the cytoplasm to be effective;[53] in contrast, accumulation in lysosomes is the goal for cancer treatments related to cell death by causing rupture of the acidic lysosome and pH-driven release of chemotherapy from the particles.[18,54]

https://doi.org/10.1021/acsanm.3c03451
ACS Appl. Nano Mater. 2023, 6, 18967−18977

We show that SNPs fabricated using methods to produce 65, 78, and 130 nm particle sizes are taken up in GBM cells after 4 h of incubation, and SNPs mostly colocalize with the lysosomes, demonstrating the potential of the SNPs being used for the lysosomal delivery of cargos. Interestingly, in all trial particle sizes, some SNPs were observed in areas of the cells that were not the lysosomes or endosomes, showing the potential of these particle systems to be utilized for cytosolic delivery with improved engineering to specifically deliver the particles to the cytoplasm. We also show that the 130 nm SNPs have a higher degree of internalization at 4 h than the 65 nm SNPs; however, more work must be done to elucidate these results further.

Developing nanocarriers for drug delivery to the central nervous system (CNS) remains a major goal toward the treatment of CNS-related diseases, such as glioblastoma multiforme (GBM), the most common primary CNS tumor in adults.[55] These tumors often develop drug resistance, while a major contributor to poor patient survival is also the challenge of delivering therapeutics across the blood−brain barrier (BBB). The role of the BBB is to restrict entry of substances between the peripheral circulation and the CNS; thus, generally only lipophilic drugs with a molecular weight <500 Da can cross the BBB, ruling out the majority of potential drug candidates. Using nanotechnology to deliver various active pharmaceutical ingredients (APIs) to the brain, in particular GBM, has gained considerable research focus[55,56] in the last few decades, as it has the potential to target specific areas of the brain and reduce adverse side effects that are associated with off-target API distribution. Thus, we conjugated anti-EGFR to the surface of SNPs, as EGFR gene amplification and overexpression are seen in 40−50% of the GBMs,[57,58] making it a promising target for future use, and EGFR-specific antibodies cetuximab and panitumumab are widely being used in treatments against metastatic colorectal cancers already.[59] Nanotechnology can also be utilized for delivering APIs that normally do not pass the BBB into the brain, such as doxorubicin,[60] which has been reported to have superior cytotoxic effects with GBM cell lines[61] over the currently used BBB penetrable drug, Temozolomide.[62] The investigation of nanoprecipitated SNPs for the potential treatment of GBM, based on lysosomal uptake in GBM cells, successful doxorubicin entrapment, and conjugation of anti-EGFR, suggests potential for future use of these particles for local delivery after maximal tumor resection or potentially even BBB penetration and GBM targeting with further optimization. Future work will assess the behavior of these functionalized particles in cellular studies with protein corona delineation.

CONCLUSIONS

Methods to control the size and surface characteristics of nanoprecipitated SNPs were investigated to provide improved control of the size and dispersity. In addition, DOX-loaded SNPs were evaluated to show potential utility in sustained release for cancer drug delivery. New understanding of the cellular uptake of these particles into cancer cells was gained by using GBM cells. The hypothesis is that these new protein nanoparticles with tight control of size, charge, and delivery options should propel further studies into their utility in a range of biomedical needs. These needs may include targeted GBM chemotherapy treatment (as seen in this work), vaccines, infection, pain management, bone disease and regeneration, and other medical conditions. Overall, biocompatible and slowly degrading biomaterial systems such as those studied here offer many areas of potential impact into the future as targeted functionalized versions are pursued.

ASSOCIATED CONTENT

Supporting Information

The Supporting Information is available free of charge at https://pubs.acs.org/doi/10.1021/acsanm.3c03451.

Images of particle solutions, EGFR antibody conjugation on ESNPs, and loading efficiency (PDF)

AUTHOR INFORMATION

Corresponding Author

David L. Kaplan − *Department of Biomedical Engineering, Tufts University, Medford, Massachusetts 02155, United States;* orcid.org/0000-0002-9245-7774; Email: david.kaplan@tufts.edu

Authors

Sawnaz Shaidani − *Department of Biomedical Engineering, Tufts University, Medford, Massachusetts 02155, United States*

Charlotte Jacobus − *Department of Biomedical Engineering, Tufts University, Medford, Massachusetts 02155, United States*

Jugal Kishore Sahoo − *Department of Biomedical Engineering, Tufts University, Medford, Massachusetts 02155, United States;* orcid.org/0000-0003-2503-9115

Kristin Harrington − *Department of Biomedical Engineering, Tufts University, Medford, Massachusetts 02155, United States*

Hannah Johnson − *Department of Chemistry and Biochemistry, San Diego State University, San Diego, California 92182-1030, United States*

Olivia Foster − *Department of Biomedical Engineering, Tufts University, Medford, Massachusetts 02155, United States*

Shangyuan Cui − *Department of Biomedical Engineering, Tufts University, Medford, Massachusetts 02155, United States*

Onur Hasturk − *Department of Biomedical Engineering, Tufts University, Medford, Massachusetts 02155, United States;* orcid.org/0000-0002-0030-8967

Thomas Falcucci − *Department of Biomedical Engineering, Tufts University, Medford, Massachusetts 02155, United States*

Ying Chen − *Department of Biomedical Engineering, Tufts University, Medford, Massachusetts 02155, United States;* orcid.org/0000-0002-9693-6668

Madison Fletcher − *Department of Biomedical Engineering, Tufts University, Medford, Massachusetts 02155, United States*

Carolynn Brooks − *Department of Biomedical Engineering, Tufts University, Medford, Massachusetts 02155, United States*

Gregory P. Holland − *Department of Chemistry and Biochemistry, San Diego State University, San Diego, California 92182-1030, United States*

Complete contact information is available at: https://pubs.acs.org/10.1021/acsanm.3c03451

Notes

The authors declare no competing financial interest.

https://doi.org/10.1021/acsanm.3c03451
ACS Appl. Nano Mater. 2023, 6, 18967−18977

■ ACKNOWLEDGMENTS

The authors thank the NIH (P41EB027062), the AFOSR (FA9550-20-1-0363; DK), and (FA9550-20-1-0103; GH) for support of these studies. The authors would also like to thank Liam Power Harrington for imaging help, Ryan Scheel for helping kickstart this work, Emily Hartzell for her inputs in intracellular imaging, and Madeleine Yost, Sabrina Zhang, Olivia Zeiden, and Elysia Chang for their contributions to the antibody conjugation methods. This work was performed in part at the Harvard University Center for Nanoscale Systems (CNS), a member of the National Nanotechnology Coordinated Infrastructure Network (NNCI).

■ REFERENCES

(1) Anselmo, A. C.; Mitragotri, S. Nanoparticles in the clinic: An update. *Bioeng. Transl. Med.* **2019**, *4* (3), No. e10143.
(2) Mitchell, M. J.; Billingsley, M. M.; Haley, R. M.; Wechsler, M. E.; Peppas, N. A.; Langer, R. Engineering precision nanoparticles for drug delivery. *Nat. Rev. Drug Discovery* **2021**, *20* (2), 101−124.
(3) Arias, L. S.; Pessan, J. P.; Vieira, A. P. M.; Lima, T. M. T.; Delbem, A. C. B.; Monteiro, D. R. Iron Oxide Nanoparticles for Biomedical Applications: A Perspective on Synthesis, Drugs, Antimicrobial Activity, and Toxicity. *Antibiotics* **2018**, *7* (2), No. 46.
(4) Szwed, M.; Torgersen, M. L.; Kumari, R. V.; Yadava, S. K.; Pust, S.; Iversen, T. G.; Skotland, T.; Giri, J.; Sandvig, K. Biological response and cytotoxicity induced by lipid nanocapsules. *J. Nanobiotechnol.* **2020**, *18* (1), No. 5.
(5) Hou, X.; Zaks, T.; Langer, R.; Dong, Y. Lipid nanoparticles for mRNA delivery. *Nat. Rev. Mater.* **2021**, *6* (12), 1078−1094.
(6) Nefzger, M.; Kreuter, J.; Voges, R.; Liehl, E.; Czok, R. Distribution and Elimination of Polymethyl Methacrylate Nanoparticles After Peroral Administration to Rats. *J. Pharm. Sci.* **1984**, *73* (9), 1309−1311.
(7) Jani, P.; Halbert, G. W.; Langridge, J.; Florence, A. T. Nanoparticle Uptake by the Rat Gastrointestinal Mucosa: Quantitation and Particle Size Dependency. *J. Pharm. Pharmacol.* **2011**, *42* (12), 821−826.
(8) Gagliardi, A.; Giuliano, E.; Venkateswararao, E.; Fresta, M.; Bulotta, S.; Awasthi, V.; Cosco, D. Biodegradable Polymeric Nanoparticles for Drug Delivery to Solid Tumors. *Front. Pharmacol.* **2021**, *12*, No. 601626.
(9) Hwang, J.; Choi, D.; Han, S.; Jung, S. Y.; Choi, J.; Hong, J. Potential toxicity of polystyrene microplastic particles. *Sci. Rep.* **2020**, *10* (1), No. 7391.
(10) Mahadevan, G.; Valiyaveettil, S. Understanding the interactions of poly(methyl methacrylate) and poly(vinyl chloride) nanoparticles with BHK-21 cell line. *Sci. Rep.* **2021**, *11* (1), No. 2089.
(11) Habibi, N.; Mauser, A.; Ko, Y.; Lahann, J. Protein Nanoparticles: Uniting the Power of Proteins with Engineering Design Approaches. *Adv. Sci.* **2022**, *9* (8), No. 2104012.
(12) Guo, C.; Li, C.; Kaplan, D. L. Enzymatic Degradation of *Bombyx mori* Silk Materials: A Review. *Biomacromolecules* **2020**, *21* (5), 1678−1686.
(13) Su, S.; Kang, P. M. Systemic Review of Biodegradable Nanomaterials in Nanomedicine. *Nanomaterials* **2020**, *10* (4), No. 656.
(14) Zhao, M.; Lei, C.; Yang, Y.; Bu, X.; Ma, H.; Gong, H.; Liu, J.; Fang, X.; Hu, Z.; Fang, Q. Abraxane, the Nanoparticle Formulation of Paclitaxel Can Induce Drug Resistance by Up-Regulation of P-gp. *PLoS One* **2015**, *10* (7), No. e0131429.
(15) Lepeltier, E.; Bourgaux, C.; Couvreur, P. Nanoprecipitation and the "Ouzo effect": Application to drug delivery devices. *Adv. Drug Delivery Rev.* **2014**, *71*, 86−97, DOI: 10.1016/j.addr.2013.12.009.
(16) Nowak, M.; Brown, T. D.; Graham, A.; Helgeson, M. E.; Mitragotri, S. Size, shape, and flexibility influence nanoparticle transport across brain endothelium under flow. *Bioeng. Transl. Med.* **2020**, *5* (2), No. e10153.
(17) Ikeda-Imafuku, M.; Wang, L.L.-W.; Rodrigues, D.; Shaha, S.; Zhao, Z.; Mitragotri, S. Strategies to improve the EPR effect: A mechanistic perspective and clinical translation. *J. Controlled Release* **2022**, *345*, 512−536.
(18) Wongpinyochit, T.; Johnston, B. F.; Seib, F. P. Manufacture and Drug Delivery Applications of Silk Nanoparticles. *J. Visualized Exp.* **2016**, No. 116, No. e54669, DOI: 10.3791/54669.
(19) Wu, J.; Sahoo, J. K.; Li, Y.; Xu, Q.; Kaplan, D. L. Challenges in delivering therapeutic peptides and proteins: A silk-based solution. *J. Controlled Release* **2022**, *345*, 176−189.
(20) Wang, X.; Yucel, T.; Lu, Q.; Hu, X.; Kaplan, D. L. Silk nanospheres and microspheres from silk/pva blend films for drug delivery. *Biomaterials* **2010**, *31* (6), 1025−1035, DOI: 10.1016/j.biomaterials.2009.11.002.
(21) Kim, S. Y.; Naskar, D.; Kundu, S. C.; Bishop, D. P.; Doble, P. A.; Boddy, A. V.; Chan, H. K.; Wall, I. B.; Chrzanowski, W. Formulation of Biologically-Inspired Silk-Based Drug Carriers for Pulmonary Delivery Targeted for Lung Cancer. *Sci. Rep.* **2015**, *5*, No. 11878.
(22) Xiao, L.; Lu, G.; Lu, Q.; Kaplan, D. L. Direct Formation of Silk Nanoparticles for Drug Delivery. *ACS Biomater. Sci. Eng.* **2016**, *2* (11), 2050−2057, DOI: 10.1021/acsbiomaterials.6b00457.
(23) Solomun, J. I.; Totten, J. D.; Wongpinyochit, T.; Florence, A. J.; Seib, F. P. Manual Versus Microfluidic-Assisted Nanoparticle Manufacture: Impact of Silk Fibroin Stock on Nanoparticle Characteristics. *ACS Biomater. Sci. Eng.* **2020**, *6* (5), 2796−2804, DOI: 10.1021/acsbiomaterials.0c00202.
(24) Salatin, S.; Barar, J.; Barzegar-Jalali, M.; Adibkia, K.; Kiafar, F.; Jelvehgari, M. Development of a nanoprecipitation method for the entrapment of a very water soluble drug into Eudragit RL nanoparticles. *Res. Pharm. Sci.* **2017**, *12* (1), 1−14.
(25) Sahin, A.; Esendagli, G.; Yerlikaya, F.; Caban-Toktas, S.; Yoyen-Ermis, D.; Horzum, U.; Aktas, Y.; Khan, M.; Couvreur, P.; Capan, Y. A small variation in average particle size of PLGA nanoparticles prepared by nanoprecipitation leads to considerable change in nanoparticles' characteristics and efficacy of intracellular delivery. *Artif. Cells, Nanomed., Biotechnol.* **2017**, *45* (8), 1657−1664, DOI: 10.1080/21691401.2016.1276924.
(26) Khramtsov, P.; Burdina, O.; Lazarev, S.; Novokshonova, A.; Bochkova, M.; Timganova, V.; Kiselkov, D.; Minin, A.; Zamorina, S.; Rayev, M. Modified Desolvation Method Enables Simple One-Step Synthesis of Gelatin Nanoparticles from Different Gelatin Types with Any Bloom Values. *Pharmaceutics* **2021**, *13* (10), No. 1537.
(27) Carvalho, J. A.; Abreu, A. S.; Ferreira, V. T. P.; Gonçalves, E. P.; Tedesco, A. C.; Pinto, J. G.; Ferreira-Strixino, J.; Beltrame Junior, M.; Simioni, A. R. Preparation of gelatin nanoparticles by two step desolvation method for application in photodynamic therapy. *J. Biomater. Sci., Polym. Ed.* **2018**, *29* (11), 1287−1301.
(28) Luque-Alcaraz, A. G.; Lizardi-Mendoza, J.; Goycoolea, F. M.; Higuera-Ciapara, I.; Argüelles-Monal, W. Preparation of chitosan nanoparticles by nanoprecipitation and their ability as a drug nanocarrier. *RSC Adv.* **2016**, *6* (64), 59250−59256.
(29) Tarhini, M.; Pizzoccaro, A.; Benlyamani, I.; Rebaud, C.; Greige-Gerges, H.; Fessi, H.; Elaissari, A.; Bentaher, A. Human serum albumin nanoparticles as nanovector carriers for proteins: Application to the antibacterial proteins "neutrophil elastase" and "secretory leukocyte protease inhibitor. *Int. J. Pharm.* **2020**, *579*, No. 119150.
(30) Seib, F. P.; Jones, G. T.; Rnjak-Kovacina, J.; Lin, Y.; Kaplan, D. L. pH-dependent anticancer drug release from silk nanoparticles. *Adv. Healthcare Mater.* **2013**, *2* (12), 1606−1611, DOI: 10.1002/adhm.201300034.
(31) Matthew, S. A. L.; Totten, J. D.; Phuagkhaopong, S.; Egan, G.; Witte, K.; Perrie, Y.; Seib, F. P. Silk Nanoparticle Manufacture in Semi-Batch Format. *ACS Biomater. Sci. Eng.* **2020**, *6* (12), 6748−6759.
(32) Pritchard, E. M.; Hu, X.; Finley, V.; Kuo, C. K.; Kaplan, D. L. Effect of silk protein processing on drug delivery from silk films. *Macromol. Biosci.* **2013**, *13* (3), 311−320.

(33) Daeihamed, M.; Haeri, A.; Dadashzadeh, S. A Simple and Sensitive HPLC Method for Fluorescence Quantitation of Doxorubicin in Micro-volume Plasma: Applications to Pharmacokinetic Studies in Rats. *Iran J. Pharm. Res.* **2015**, *14*, 33−42.
(34) Hasturk, O.; Sahoo, J. K.; Kaplan, D. L. Synthesis and Characterization of Silk Ionomers for Layer-by-Layer Electrostatic Deposition on Individual Mammalian Cells. *Biomacromolecules* **2020**, *21* (7), 2829−2843.
(35) Lu, Q.; Wang, X.; Zhu, H.; Kaplan, D. L. Surface immobilization of antibody on silk fibroin through conformational transition. *Acta Biomater.* **2011**, *7* (7), 2782−2786, DOI: 10.1016/j.actbio.2011.03.001.
(36) Wang, X.; Kluge, J. A.; Leisk, G. G.; Kaplan, D. L. Sonication-induced gelation of silk fibroin for cell encapsulation. *Biomaterials* **2008**, *29* (8), 1054−1064, DOI: 10.1016/j.biomaterials.2007.11.003.
(37) Kaewprasit, K.; Kobayashi, T.; Damrongsakkul, S. Thai silk fibroin gelation process enhancing by monohydric and polyhydric alcohols. *Int. J. Biol. Macromol.* **2018**, *118*, 1726−1735.
(38) Hu, X.; Shmelev, K.; Sun, L.; Gil, E. S.; Park, S. H.; Cebe, P.; Kaplan, D. L. Regulation of silk material structure by temperature-controlled water vapor annealing. *Biomacromolecules* **2011**, *12* (5), 1686−1696.
(39) Matthew, S. A. L.; Rezwan, R.; Perrie, Y.; Seib, F. P. Volumetric Scalability of Microfluidic and Semi-Batch Silk Nanoprecipitation Methods. *Molecules* **2022**, *27* (7), No. 2368.
(40) Matthew, S. A. L.; Totten, J. D.; Phuagkhaopong, S.; Egan, G.; Witte, K.; Perrie, Y.; Seib, F. P. Silk Nanoparticle Manufacture in Semi-Batch Format. *ACS Biomater. Sci. Eng.* **2020**, *6* (12), 6748−6759.
(41) Sandra, F.; Khaliq, N. U.; Sunna, A.; Care, A. Developing Protein-Based Nanoparticles as Versatile Delivery Systems for Cancer Therapy and Imaging. *Nanomaterials* **2019**, *9* (9), No. 1329.
(42) Pustulka, S. M.; Ling, K.; Pish, S. L.; Champion, J. A. Protein Nanoparticle Charge and Hydrophobicity Govern Protein Corona and Macrophage Uptake. *ACS Appl. Mater. Interfaces* **2020**, *12* (43), 48284−48295.
(43) Fountain, J. N.; Hawker, M. J.; Hartle, L.; Wu, J.; Montanari, V.; Sahoo, J. K.; Davis, L. M.; Kaplan, D. L.; Kumar, K. Towards Non-stick Silk: Tuning the Hydrophobicity of Silk Fibroin Protein. *ChemBioChem* **2022**, *23*, No. e202200429.
(44) Forest, V.; Cottier, M.; Pourchez, J. Electrostatic interactions favor the binding of positive nanoparticles on cells: A reductive theory. *Nano Today* **2015**, *10* (6), 677−680.
(45) Wongpinyochit, T.; Totten, J. D.; Johnston, B. F.; Seib, F. P. Microfluidic-assisted silk nanoparticle tuning. *Nanoscale Adv.* **2019**, *1* (2), 873−883.
(46) Lammel, A.; Schwab, M.; Slotta, U.; Winter, G.; Scheibel, T. Processing Conditions for the Formation of Spider Silk Microspheres. *ChemSusChem* **2008**, *1* (5), 413−416.
(47) Florczak, A.; Jastrzebska, K.; Bialas, W.; Mackiewicz, A.; Dams-Kozlowska, H. Optimization of spider silk sphere formation processing conditions to obtain carriers with controlled characteristics. *J. Biomed. Mater. Res., Part A* **2018**, *106* (12), 3211−3221.
(48) Lai, S. K.; O'Hanlon, D. E.; Harrold, S.; Man, S. T.; Wang, Y. Y.; Cone, R.; Hanes, J. Rapid transport of large polymeric nanoparticles in fresh undiluted human mucus. *Proc. Natl. Acad. Sci. U.S.A.* **2007**, *104* (5), 1482−1487.
(49) Hua, S. Physiological and Pharmaceutical Considerations for Rectal Drug Formulations. *Front. Pharmacol.* **2019**, *10*, No. 1196.
(50) Sandri, G.; Bonferoni, M. C.; Ferrari, F.; Rossi, S.; Caramella, C. M. The Role of Particle Size in Drug Release and Absorption. In *Particulate Products: Tailoring Properties for Optimal Performance*; Merkus, H. G.; Meesters, G. M. H., Eds.; Springer International Publishing: Cham, 2014; pp 323−341.
(51) Florczak, A.; Grzechowiak, I.; Deptuch, T.; Kucharczyk, K.; Kaminska, A.; Dams-Kozlowska, H. Silk Particles as Carriers of Therapeutic Molecules for Cancer Treatment. *Materials* **2020**, *13* (21), No. 4946.
(52) Barua, S.; Mitragotri, S. Challenges associated with Penetration of Nanoparticles across Cell and Tissue Barriers: A Review of Current Status and Future Prospects. *Nano Today* **2014**, *9* (2), 223−243.
(53) Wu, Z.; Li, T. Nanoparticle-Mediated Cytoplasmic Delivery of Messenger RNA Vaccines: Challenges and Future Perspectives. *Pharm. Res.* **2021**, *38* (3), 473−478, DOI: 10.1007/s11095-021-03015-x.
(54) Qiu, J.; Xia, Y. Killing cancer cells by rupturing their lysosomes. *Nat. Nanotechnol.* **2020**, *15* (4), 252−253.
(55) Michael, J. S.; Lee, B. S.; Zhang, M.; Yu, J. S. Nanotechnology for Treatment of Glioblastoma Multiforme. *J. Transl. Intern. Med.* **2018**, *6* (3), 128−133.
(56) Patel, T.; Zhou, J.; Piepmeier, J. M.; Saltzman, W. M. Polymeric nanoparticles for drug delivery to the central nervous system. *Adv. Drug Delivery Rev.* **2012**, *64* (7), 701−705, DOI: 10.1016/j.addr.2011.12.006.
(57) Guo, G.; Gong, K.; Beckley, N.; Zhang, Y.; Yang, X.; Chkheidze, R.; Hatanpaa, K. J.; Garzon-Muvdi, T.; Koduru, P.; Nayab, A.; Jenks, J.; Sathe, A. A.; Liu, Y.; Xing, C.; Wu, S.-Y.; Chiang, C.-M.; Mukherjee, B.; Burma, S.; Wohlfeld, B.; Patel, T.; Mickey, B.; Abdullah, K.; Youssef, M.; Pan, E.; Gerber, D. E.; Tian, S.; Sarkaria, J. N.; McBrayer, S. K.; Zhao, D.; Habib, A. A. EGFR ligand shifts the role of EGFR from oncogene to tumour suppressor in EGFR-amplified glioblastoma by suppressing invasion through BIN3 upregulation. *Nat. Cell Biol.* **2022**, *24* (8), 1291−1305.
(58) Hatanpaa, K. J.; Burma, S.; Zhao, D.; Habib, A. A. Epidermal growth factor receptor in glioma: signal transduction, neuropathology, imaging, and radioresistance. *Neoplasia* **2010**, *12* (9), 675−684.
(59) García-Foncillas, J.; Sunakawa, Y.; Aderka, D.; Wainberg, Z.; Ronga, P.; Witzler, P.; Stintzing, S. Distinguishing Features of Cetuximab and Panitumumab in Colorectal Cancer and Other Solid Tumors. *Front. Oncol.* **2019**, *9*, No. 849, DOI: 10.3389/fonc.2019.00849.
(60) Shi, W.; Cui, X.; Shi, J.; Chen, J.; Wang, Y. Overcoming the blood−brain barrier for glioma-targeted therapy based on an interleukin-6 receptor-mediated micelle system. *RSC Adv.* **2017**, *7* (44), 27162−27169.
(61) Sardi, I.; Fantappiè, O.; la Marca, G.; Giovannini, M. G.; Iorio, A. L.; da Ros, M.; Malvagia, S.; Cardellicchio, S.; Giunti, L.; de Martino, M.; Mazzanti, R. Delivery of doxorubicin across the blood−brain barrier by ondansetron pretreatment: a study in vitro and in vivo. *Cancer Lett.* **2014**, *353* (2), 242−247.
(62) Iorio, A. L.; Da Ros, M.; Pisano, C.; de Martino, M.; Genitori, L.; Sardi, I. Combined Treatment with Doxorubicin and Rapamycin is Effective against In Vitro and In Vivo Models of Human Glioblastoma. *J. Clin. Med.* **2019**, *8* (3), No. 331.

https://doi.org/10.1021/acsanm.3c03451
ACS Appl. Nano Mater. 2023, 6, 18967−18977